

Ab initio atom–atom potentials using CAMCASP: Many-body potentials for the pyridine dimer.

Alston J. Misquitta¹ and Anthony J. Stone²

¹*School of Physics and Astronomy, Queen Mary, University of London, London E1 4NS, U.K.**

²*University Chemical Laboratory, Lensfield Road, Cambridge, CB2 1EW, U.K.*

(Dated: February 28, 2022)

In Part I of this two-part investigation we described a methodology for the development of robust, analytic, many-body atom–atom potentials for small organic molecules from first principles and demonstrated how the CAMCASP program can be used to derive the damped, distributed multipole models for pyridine. Here we demonstrate how the theoretical ideas for the short-range models described in Part I, which are implemented in the CAMCASP suite of programs, can be used to develop a series of many-body potentials for the pyridine system. Even the simplest of these potentials exhibit r.m.s. errors of only about 0.6 kJ mol^{-1} for the low-energy pyridine dimers, significantly surpassing the best empirical potentials. Our best model is shown to support eight stable minima, four of which have not been reported in the literature before. Further, the functional form can be made systematically more elaborate so as to improve the accuracy without a significant increase in the human-time spent in their generation. We investigate the effects of anisotropy, rank of multipoles, and choice of polarizability and dispersion models.

PACS numbers:

I. INTRODUCTION

In Part I we introduced our strategy for developing accurate, analytic, many-body potentials for molecular systems in manner that is both robust and easy to implement. The key ideas of this strategy included the following: (1) that all of the long-range potential parameters are derived from the density and density response functions; (2) that the short-range parameters, including the atomic shape anisotropy, are obtained via the distributed density-overlap model with a partitioning scheme based on the iterated stockholder atom (ISA) approach [1, 2]; (3) that we derive the potential in stages, with parameters derived or fitted at each stage used as prior values for the next stage. Uniquely in our scheme, the ISA density-partitioning method plays a central role in the potential development process; in particular, the ISA is key to the robustness of the methodology used to determine the short-range parameters, which pose a significant problem for standard fitting methods. We have based our approach on the basis-space ISA, or BS-ISA, algorithm [3] that allows us to partition a molecular density uniquely into atomic domains and obtain analytic expansions for the ISA atoms. The BS-ISA algorithm has many desirable properties that make it ideal for our purpose [3]: there is a well-defined basis-set limit to the ISA atoms; the distributed multipole moments resulting from this partitioning have been shown to be amongst the most rapidly converging with rank; and the ISA atoms are, in an information-theoretic sense, the most spherical atoms possible that simultaneously take into account atomic electronegativity changes in the molecule. It is because of these properties that we expect the short-range potential parameters to be physical and well-defined.

In this paper we will apply the methodology presented in Part I to develop a set of many-body potentials for pyridine.

In a study such as this is, it is important to use a system that simultaneously presents a challenge and also allows tests to be performed to validate the method sufficiently. We have chosen to use the pyridine dimer as our example as it is small enough to permit accurate interaction energy calculations using SAPT(DFT) on as dense a grid as is needed, but large enough to exhibit a varied and complex potential energy surface (PES) with—as we shall see below—eight distinct minima. Additionally, the pyridine molecule has a sizeable dipole moment and polarizability, so polarization effects are expected to be important, and, as we shall see, the two-body charge-transfer, or charge-delocalisation [4], energy is also significant. Finally, from the crystallographic studies by Price and co-workers [5] it is known that the crystal energy landscape of this molecule is complex and poses a significant challenge for seemingly accurate empirical potentials. While we will not attempt to use the results of this study in a crystal structure prediction, we intend to perform this test in later work.

This paper is organised as follows: we begin with a description of the numerical details of the electronic structure calculations used in this work and a description of the data sets used in the potential development process. Next, in §III we develop a set of short-range models which are then combined with the long-range models derived in Part I in §IV. The resulting total energy potentials are analysed in §V where we compare pyridine dimer minima, vibrational frequencies and the second virial coefficients on these surfaces. In §VI we critically analyse aspects of the methodology and the potentials. In particular, we examine the stability of the potentials with respect to multipole rank. In the Conclusions we examine shortcomings of the method and indicate possible directions for this work.

II. NUMERICAL DETAILS

The numerical details related to the distributed multipole models and SAPT(DFT) calculations are described in §4 in

*Electronic address: a.j.misquitta@qmul.ac.uk

Part I. There we also describe the three data sets used in the development of the pyridine potentials. Here we provide additional numerical details related to the weighting schemes used in the fitting process.

The distributed density-overlap fits were performed using the CAMCASP program using the Gaussian/Log weighting scheme [6] in which $w_{\text{GL}}(e) = \exp(-\alpha(\ln(e/E_0))^2)$, where $\alpha = 1/\ln 10$ and $E_0 = 100 \text{ kJ mol}^{-1}$. Here the parameter E_0 sets the energy-scale for the fit, and it is usually chosen to be some large multiple of the absolute global minimum dimer energy so as to obtain a reliable fit to the repulsive wall. The fits to individual site-site potentials $V_{\text{sr}}[ab]$ were performed with the ORIENT program using the same Gaussian/Log weighting scheme.

All relaxation steps were performed using the ORIENT program using the Boltzmann weighting function

$$w_{\text{Bol}}(e) = \begin{cases} \exp((e_{\text{low}} - e)/E_0) & \text{for } e > e_{\text{low}} \\ 1.0 & \text{otherwise.} \end{cases} \quad (1)$$

Here e_{low} is typically set to the smallest energy in the data set and the energy-scale for the fit is set by $E_0 = 40 \text{ kJ mol}^{-1}$ to increase the weight to lower energies. We used $e_{\text{low}} = 0 \text{ kJ mol}^{-1}$ for the relaxation of the repulsive energies, and -10 kJ mol^{-1} in the final relaxation step involving the total interaction model.

III. SHORT-RANGE FIT

A. Fitting strategy and atomic shape

We set out the fitting strategy for the short-range part of the potential in some detail in §3 of Part I. In this multi-stage approach we first fit to $E_{\text{sr}}^{(1)}$ calculated on the dense, pseudo-random set of 3515 dimers in Dataset(0). This is done via the distributed density-overlap model which allows us to partition $E_{\text{sr}}^{(1)}$ into contributions from pairs of sites, and fit the terms in the potential for each atom-pair individually. However, if the atoms are close to spherical, as is the case for the ISA atom densities, the atom-pair shape function $\rho_{ab}(\Omega_{ab})$ that appears in the potential (see eq. (5) in Part I) may be written to a good approximation as the sum of shape functions for the interacting atoms (see ch. 12 in ref. 7)

$$\rho_{ab}(\Omega_{ab}) \approx \rho_a(\Omega_a) + \rho_b(\Omega_b). \quad (2)$$

Here Ω_a is a generalised angular coordinate that describes the direction of the vector from site a to site b in the local coordinate system of site a , and likewise for Ω_b , and ρ_a and ρ_b are the atomic shape functions for atoms a and b . The atomic shape functions for all atoms of a given type should be the same.

The shape-function additivity is observed in the first stage of the fitting when the terms in $V_{\text{sr}}^{(1)}[ab]$ are fitted individually via the density-overlap model, but it is not exact, probably in part because of grid sampling variability around the sites. It can however be exactly enforced in the next stage when

the short-range parameters are collectively relaxed in a constrained manner to the $E_{\text{sr}}^{(1)}$ energies in Dataset(1). We find it best to perform this relaxation iteratively, with only those parameters associated with a particular subset of sites relaxed at each step. With this approach the constrained relaxation can be performed rapidly, in a computationally efficient manner. At each step, shape-function additivity is imposed by using pinning (prior) values for the parameters from the averaged shape-function parameters from the previous step.

In a similar manner, we may relax the resulting potential parameters to include effects from second and higher orders in the interaction operator. However, there is no reason to expect the shape-function additivity to hold at this stage, as the higher-order short-range effect, which is predominantly the charge-transfer (or charge-delocalisation) energy, depends on the pair of atoms involved in a non-additive manner. In the absence of additivity, the number of independent parameters in the potential would depend quadratically on the number of interacting atoms, but fortunately, as we will demonstrate below, the higher-order correction can be treated as isotropic. That is, the atom-pair shape function now becomes

$$\rho_{ab}(\Omega_{ab}) = \rho_a(\Omega_a) + \rho_b(\Omega_b) - \delta_{ab}, \quad (3)$$

where δ_{ab} is the isotropic higher-order correction.

We will now examine the effectiveness of this strategy in obtaining a series of fits to the short-range potential for the pyridine dimer.

B. Fitting using the distributed density overlap model

In principle, it is straightforward to use the distributed density-overlap model described above. We have used this approach [8, 9], as have others [6, 10–12], with a reasonable degree of success. The problem lies in the choice of density partitioning method. There is no unique way of decomposing a density into atom-like domains, yet the tacit assumption of the distributed density-overlap model is that the partitioned density ρ_a^A is well-behaved and may be used to extract properties such as size and shape of the atom located on site a . If this were not the case, then the potential parameters extracted from the model would be meaningless, and indeed, a fit to eq. (11) in Part I could even be so poor as to be useless. In the past we have used a density-fitting-based scheme to partition the density [8]. This works by expressing the electronic density as a single sum over an auxiliary basis set with functions located on the atomic nuclei, which then naturally suggests a partitioning scheme:

$$\begin{aligned} \rho(\mathbf{r}) &= \sum_k d_k \chi_k(\mathbf{r}) \\ &= \sum_a \sum_{k \in a} d_k \chi_k(\mathbf{r}) = \sum_a \rho_a(\mathbf{r}). \end{aligned} \quad (4)$$

Here the d_k are expansion coefficients and χ_k are Gaussian basis functions from the auxiliary basis. We have previously argued [13] that since the auxiliary basis sets are optimised on free atoms, or homo-diatoms, they may be used in the above

manner to partition the molecular density into atom-like parts. This does seem to work, but only if small enough auxiliary basis sets are used, and even then, the resulting atomic domains may be meaningless.

In Figure 1 we present the density-fitting-based (DF-based) atomic isodensity surfaces for the atoms in the pyridine molecule. The total electronic density of pyridine was obtained with the d-aug-cc-pVTZ basis using the PBE0/AC functional. We had to use the relatively less diffuse def-TZVPP basis for the density-fitting as results with any of the more diffuse RIMP2 auxiliary basis sets were so full of artifacts associated with the basis set over-completeness as to lead to completely nonsensical results for the density partitioning. However, even with the relatively small def-TZVPP basis, the DF-based density partitioning results in carbon atoms with rather unusual shapes. If this partitioning method is used to construct a short-range potential using the density-overlap model as described above, we obtain potentials with spurious terms in the atomic anisotropies and overall very poor fit qualities.

In contrast, we can see in Figure 2 that the ISA-based atomic shapes obtained using the algorithm described in §7 of Part I are very well-behaved. These have been obtained with the significantly larger aug-cc-pVQZ/ISA-set2 fitting basis and show none of the artifacts seen with the DF-based scheme. Additionally, the ISA-based atoms do not show any significant differences in shape when other basis sets are used, as long as these are large and diffuse enough. This is a significant result: if we wish the atomic shapes to be, in some sense, universal or transferable (properties we will not explore in this paper), we must be able to calculate the atomic shapes with an algorithm that possesses a well-defined basis-set limit. The ISA approach is not the only such method, but for reasons discussed in the Introduction of Part I and in ref. 3, it is one of the few partitioning methods that has desirable numerical properties while satisfying physical and chemical expectations.

In Figure 3 we present the ISA-atomic shapes viewed in the molecular plane, along the bond axis, or, in the case of the nitrogen atom, along the N \cdots C3 axis. In order to highlight the atomic anisotropies we have superimposed on the 10^{-3} a.u. isodensity surfaces some contours showing the intersection with spheres centred on the atomic nuclei. These contours clearly illustrate the shape symmetries of each of the atoms. Also included in the figure are the important shape anisotropies for these atoms. These have been calculated by fitting $E_{\text{sr}}^{(1)}$ via the distributed overlap model using a set of local axis frames located on the atomic centres with the x axis pointing along and out of the bond, and the z axis perpendicular to and pointing out of the plane of the molecule. During the relaxation step in this fit we eliminate all terms that are less than a threshold, taken to be 0.01 a.u. The picture that emerges is remarkably simple and convincing:

- *Nitrogen*: The largest anisotropy term for the nitrogen atom in pyridine is the 22c term that is associated with the lone pair. Additionally one may include the 11c and 20 terms on the nitrogen atoms, though these are smaller. All other terms are negligible.

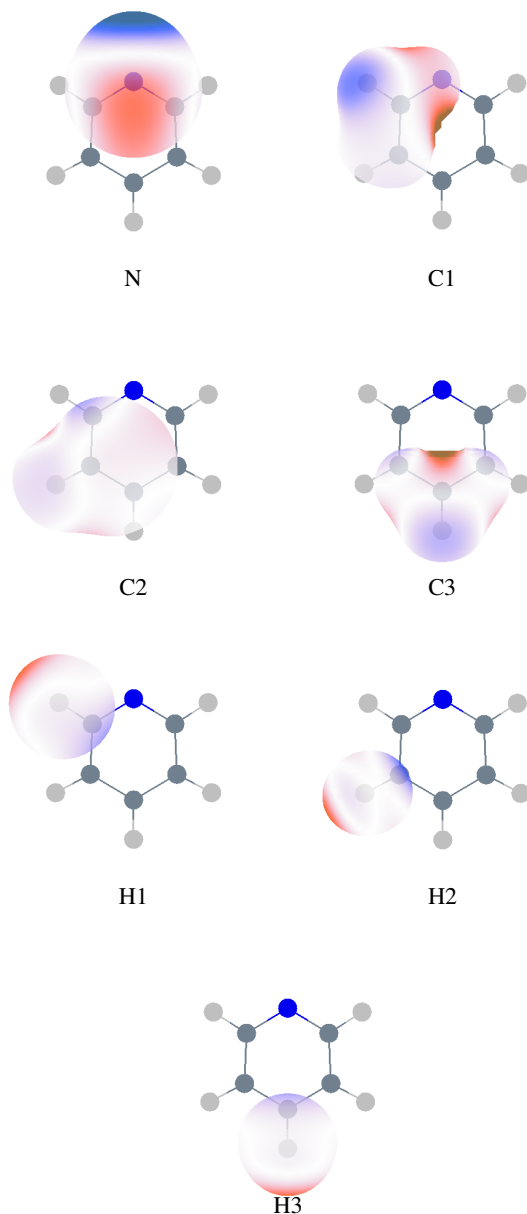


FIG. 1: The 10^{-3} a.u. iso-density surfaces of the density-fitting-based ‘atoms’ in pyridine. The pyridine density was computed using a d-aug-cc-pVTZ basis, and the density-fitting was performed using the TZVPP auxiliary basis. The colour coding indicates the anisotropic component of the electrostatic potential on the surface arising from ISA-based atomic multipoles located on the nuclei; that is, the atomic charge contributions are not included. The scale used varies from -0.5 V (blue), through 0 V (white), to $+0.5$ V (red).

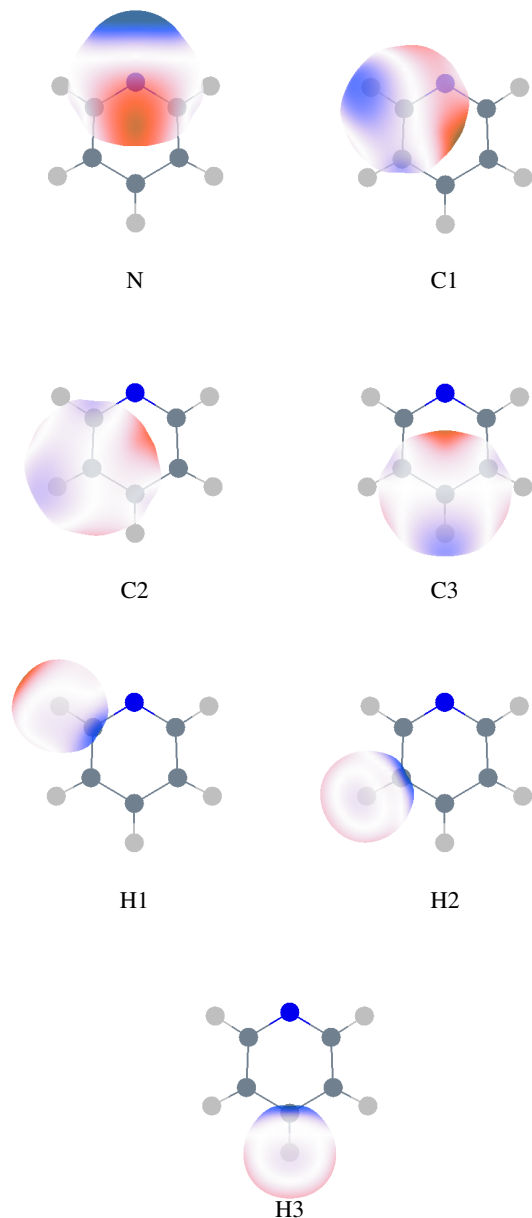


FIG. 2: The 10^{-3} a.u. iso-density surfaces of the ISA-based ‘atoms’ in pyridine. The pyridine density was computed using a d-aug-cc-pVTZ basis and the ISA calculations were performed using the aug-cc-pVQZ/ISA-set2 auxiliary basis set. Colour coding as described in Figure 1.

- *Carbon*: The 20 term associated with the p_z orbitals is the dominant source of anisotropy on all carbon atoms. Of the other symmetry-allowed terms, the 11c term associated with the C–H bond is relatively strong. The 22c terms are present, but small. Finally, C1 and C2 contain 11s terms due to the proximity of the N atom. These terms describe the in-plane distortion of the C1/C2 densities due to N.
- *Hydrogen*: We have limited all hydrogen atoms to rank 1 terms only. All hydrogen atoms possess a 11c term to describe the electronic distortion along the C–H bond and, both H1 and H2 additionally have 11s terms.

We have developed three models for the short-range terms: srModel(1) contains only isotropic terms, in srModel(2) we have included the 22c anisotropy term on the nitrogen atom, and in srModel(3) we have used all the anisotropy terms shown in Figure 3. In all three models, the hardness parameters α_{ab} in eq. (5) in Part I were kept isotropic. The constrained relaxation was performed using eq. (12) in Part I with constraint strength parameters c_i chosen to be 0.1 for the isotropic parameters and 1.0 for the anisotropic terms in the $\rho_{ab}(\Omega)$ expansions. This choice was made empirically on the basis that the appropriate parameters were those that when further reduced did not result in any appreciable improvement in the fit quality. The distributed density-overlap fits were performed using the CAMCASP program, and the fits to individual site-site potentials $V_{sr}[ab]$ were performed using the ORIENT program. The weighting schemes used in these fits are described in §II. The relaxation step was also performed using the ORIENT program but this time using the Boltzmann weighting function as described in §II. The scatter plots of these models at various stages in the fitting process are shown in Figure 4. Weighted r.m.s. errors at the final stage are 1.03, 0.90, and 0.61 kJ mol^{-1} for models 1, 2 and 3, respectively. These uncertainties are less than our target of 1 kJ mol^{-1} for all three models, but the performance of srModel(3) is quite remarkable, with errors less than or close to 1 kJ mol^{-1} for energies as large as 100 kJ mol^{-1} .

C. Infinite-order charge transfer (delocalisation) energy

The infinite-order charge-transfer energy is the dominant short-range contribution at second and higher orders in the intermolecular interaction operator. While we can use regularised SAPT(DFT) [4, 14] to determine the second-order charge-transfer energy, the contributions from higher orders cannot, at present, be computed within the SAPT framework. Unfortunately, where charge-transfer is important, these higher-order effects appear to be too large to be ignored, so we need to account for them, if only approximately. As it turns out, the discussion of the infinite-order polarization in §5.2 of Part I readily suggests an approximation. If we argue that the infinite-order induction energy is the sum of just the infinite-order charge-transfer and polarization terms (i.e., assuming that there are no cross terms present), then if we know any two, we can compute the third. Here we approximate the

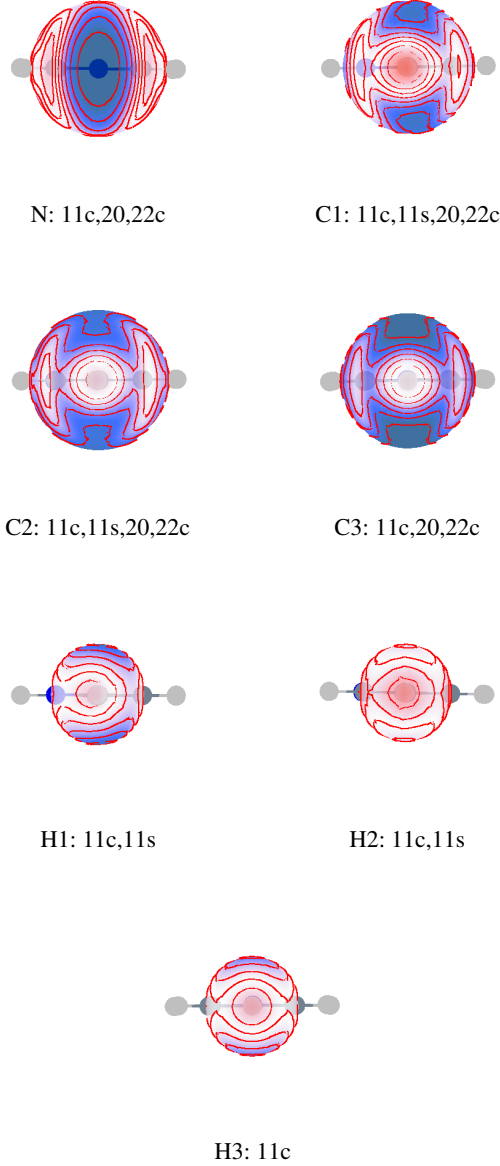


FIG. 3: Along-the-bond views of the ISA-based ‘atoms’ in pyridine. Here we illustrate the anisotropy of the atom shapes by contours showing the intersections with spherical surfaces centred at the atomic nuclei. The dominant anisotropy terms for each atom are listed for local axis frameworks with the x axis pointing out of the bond (out of the page) and the z axis normal to the plane of the molecule.

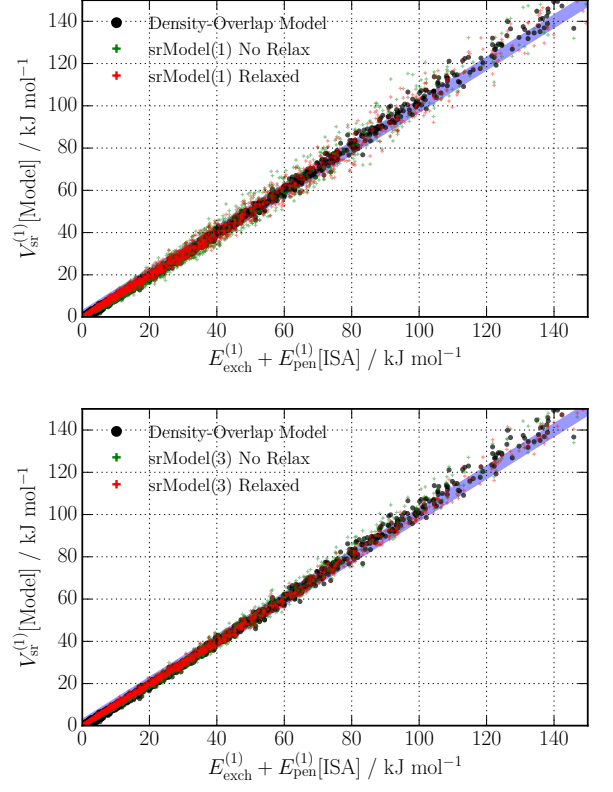


FIG. 4: Performance of two of the short-range models fitted to $E_{\text{sr}}^{(1)}$. srModel(1) is fully isotropic and srModel(3) contains the anisotropy terms described in the text and indicated in Figure 3. srModel(2) results are only slightly better than those from srModel(1) and are not shown. The black circles are results directly from the distributed density-overlap model; the green plus signs are data obtained from the model fitted to eq. (5) in Part I before relaxation, and the red plus signs are the same after relaxation to $E_{\text{sr}}^{(1)}$. The blue bar represents the $\pm 1 \text{ kJ mol}^{-1}$ range.

infinite-order induction energy as:

$$E_{\text{IND}}^{(2-\infty)} \approx E_{\text{IND}}^{(2)} + \delta_{\text{int}}^{\text{HF}} \quad (5)$$

and define the two-body infinite-order charge-transfer energy to be

$$\begin{aligned} E_{\text{CT}}^{(2-\infty)} &= E_{\text{IND}}^{(2-\infty)} - E_{\text{POL}}^{(2-\infty)} \\ &\approx E_{\text{IND}}^{(2)} + \delta_{\text{int}}^{\text{HF}} - V_{\text{pol}}^{(2-\infty)}[\text{DM}]. \end{aligned} \quad (6)$$

While this expression is readily implemented, it has a drawback in that the definition depends on the type of polarization model used.

In Figure 5 we have plotted the infinite-order charge-transfer energy calculated using eq. (6) against the first-order short-range energy $E_{\text{sr}}^{(1)}$. First of all, at about 20% of $E_{\text{sr}}^{(1)}$, $E_{\text{CT}}^{(2-\infty)}$ is a significant contribution to the short-range energy and it cannot be ignored. Second, while these two energies are roughly proportional, there is a significant scatter, particularly at the larger charge-transfer energies. Nevertheless, the

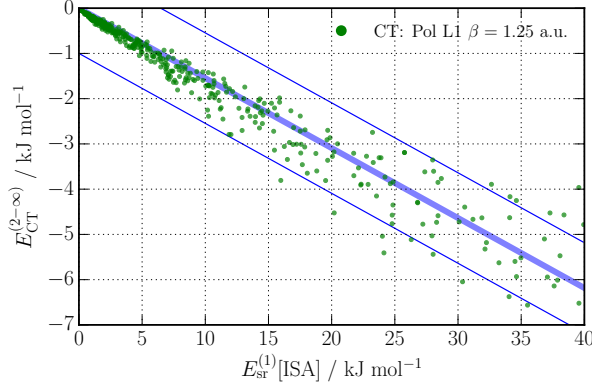


FIG. 5: The infinite-order charge delocalisation (charge-transfer) energy plotted against the first-order short-range energy $E_{\text{sr}}^{(1)}$. The thin blue lines represent the $\pm 1 \text{ kJ mol}^{-1}$ limits.

scatter is rarely more than $\pm 1 \text{ kJ mol}^{-1}$. If we argue that the charge-transfer contribution to the intermolecular interaction energy arises from a tunneling process [4], then it is natural to assume that the tunneling probability will be roughly proportional to the electron density overlap, but further work needs to be done to see whether this holds for other systems.

We may include $E_{\text{CT}}^{(2-\infty)}$ into our models for the short-range energy by constrained relaxation of the parameters in the models already obtained for $E_{\text{sr}}^{(1)}$, or we may exploit the approximate proportionality of $E_{\text{sr}}^{(1)}$ and $E_{\text{CT}}^{(2-\infty)}$ and absorb the bulk of the charge-transfer effects by scaling as follows. If we assume a proportionality with constant $k < 0$:

$$E_{\text{CT}}^{(2-\infty)} \approx k E_{\text{sr}}^{(1)} \approx k V_{\text{sr}}^{(1)}, \quad (7)$$

then we can include $E_{\text{CT}}^{(2-\infty)}$ into the short-range energy model by scaling it by $(1 - k)$ yielding

$$\begin{aligned} V_{\text{sr}}^{(1-\infty)} &\approx (1 - k) V_{\text{sr}}^{(1)} \\ &\approx (1 - k) \sum_{a,b} G \exp[-\alpha_{ab}(r_{ab} - \rho_{ab}(\Omega_{ab}))], \end{aligned} \quad (8)$$

then, re-writing $1 - k = \exp[-\alpha_{ab}\delta_{ab}]$, where $\delta_{ab} = -\ln(1 - k)/\alpha_{ab}$, we get

$$V_{\text{sr}}^{(1-\infty)} = \sum_{a,b} G \exp[-\alpha_{ab}(r_{ab} - (\rho_{ab}(\Omega_{ab}) - \delta_{ab}))]. \quad (9)$$

That is, the isotropic atom-pair radii are reduced by δ_{ab} by the attractive effects of the charge delocalisation process. The atom-pair shape-function $\rho_{ab}(\Omega_{ab})$ remains additive in the sense of eq. (2), but there is an isotropic non-additive correction δ_{ab} , as shown in eq. (3).

For the pyridine dimer we get $k \approx 0.16$ (it varies slightly with the type of polarization model used). Therefore the pair-radius reduction is of the order 0.05 Bohr, which is small but not negligible as it leads to an overall reduction in the intermolecular separation of a few tenths of a Bohr in some dimer orientations. These effects may be expected to be larger in

more strongly hydrogen-bonded systems where the charge-delocalisation is stronger.

The above scaling absorbs the bulk of the charge-transfer energy into our short-range energy models. The remainder may be included in a subsequent relaxation step, but we find that this is not necessary as it is usually small, and in any case, this and all other errors against the SAPT(DFT) reference energies will be accounted for in the final relaxation stage that we describe next.

IV. TOTAL ENERGY FITS: COMBINING THE TERMS

The analytic fits to the various components of the total interaction energy model may be combined as appropriate, and optionally relaxed, using constraints, to the total SAPT(DFT) interaction energies calculated for a suitable set of dimer geometries. These models have been obtained with a significant amount of data derived directly from the density and transition densities using various partitioning methods. The limited amount of fitting has been largely restricted to the short-range energy model, and even here, our approach ensures that the parameters are well-defined and physically meaningful, with little of the uncertainty usually associated with fits to sums of exponentials. Further, the target residual error for each of the models has been 0.5 to 1 kJ mol^{-1} , and we have largely succeeded in achieving this target. Consequently, as we shall see, these models may be combined without further relaxation to produce reasonably accurate models for the total interaction energy.

In this paper, we have reported the following models:

- *Short-range*: Three models have been obtained. srModel(1) is fully isotropic; srModel(2) contains a 22c anisotropy term on the nitrogen atoms; and srModel(3) contains all the dominant anisotropy terms needed. These short-range energy models include the first-order exchange, the electrostatic penetration, and infinite-order charge-transfer energies.
- *Electrostatic*: A rank 4 ISA-based distributed multipole model.
- *Polarization*: Three distributed polarization models obtained from the WSM procedure. The L1(iso) and L1 models include rank 1 polarizabilities, with the former being isotropic, and the L2 model includes terms to rank 2 on the heavy atoms. All these models are damped. The many-body contributions are obtained through the polarization models. We will consider only the L1 model in this paper.
- *Dispersion*: Two damped isotropic dispersion models have been obtained. The $C_6(\text{iso})$ model contains only (scaled) isotropic C_6 coefficients for all pairs of atoms. And the $C_{12}(\text{iso})$ model consists of isotropic terms to C_{12} between pairs of heavy atoms, isotropic terms to C_{10} between any hydrogen atom and a heavy atom, and only isotropic C_6 terms between pairs of hydrogen

atoms. As the C_{12} terms in the $C_{12}(\text{iso})$ are found to have a minimal effect on the quality of the model, we will instead use the equivalent $C_{10}(\text{iso})$ in the remainder of this work. All models are damped. At present we do not include any three-body dispersion non-additivity.

This gives us 18 possible ways of combining these models into total interaction energy potentials. Of these, we explore three combinations in this paper:

- *Model(1)*: Isotropic short-range model, with rank 4 ISA-DMA, L1 polarizability model, and $C_{10}(\text{iso})$ dispersion model.
- *Model(2)*: Short-range model containing isotropic terms on all atoms and an additional 22c term on the nitrogen atoms, with rank 4 ISA-DMA, L1 polarizability model, and $C_{10}(\text{iso})$ dispersion model.
- *Model(3)*: Anisotropic short-range model, combined with rank 4 ISA-DMA, L1 polarizability model, and $C_{10}(\text{iso})$ dispersion model.

These models differ only in their description of the short-range repulsion.

In Table I we report r.m.s. errors made by these models before relaxation against the SAPT(DFT) interaction energies. The r.m.s. errors are remarkably small at this stage, with models (1) and (3) exhibiting errors less than 1 kJ mol^{-1} for the most energetically important dimers. Surprisingly, Model(2) fares slightly worse than the simpler Model(1) with r.m.s. errors of 1.5 kJ mol^{-1} in this energy range. All models fare reasonably well for the positive energy dimers, with r.m.s. errors between 1.8 to 2.9 kJ mol^{-1} .

The models may be improved by constrained relaxation to SAPT(DFT) total interaction energies. We initially relaxed the models against energies from the random dimers in Dataset(1), but this led to a reduction in the quality of the fits for the test set of low-energy dimers. It appears that while the random dimers are suitable for an unbiased parametrization of the individual components of the model, they are not suitable for relaxing the sum of these components. The principal reason for this seems to be that the random dimer set does not contain low-energy dimers, as can be seen in Figure 6. Consequently, relaxing to this set causes the models to represent these relatively high-energy dimers better at the cost of the more physically important low-energy configurations. Because of this, we have performed the relaxation of the models using both Dataset(1) and Dataset(2).

The constrained relaxation was performed using the ORIENT program with the weighting scheme described in §II. Constraints were imposed using eq. (12) in Part I with tight constraint strength parameters c_i chosen to be 1.0 for the isotropic parameters and the C_8 and C_{10} parameters. The C_6 terms were kept unaltered so as to preserve the long-range dispersion interaction. The anisotropy parameters were not allowed to vary. Rather than relax all parameters simultaneously, the relaxation was performed in stages, with parameters associated with particular sites allowed to vary in each stage. This procedure,

though computationally efficient, needed to be iterated to ensure that the relaxation was adequate.

In Table I we also report r.m.s. errors made by the relaxed models. After relaxation, all three models show r.m.s. errors of only 0.5 to 0.6 kJ mol^{-1} for the most strongly bound dimers, and somewhat larger errors for the higher energy dimers. Perhaps unsurprisingly, Model(3) fares best, with r.m.s. errors less than 1 kJ mol^{-1} for all dimers with energies less than or equal to 20 kJ mol^{-1} .

In Figure 6 we display scatter plots of the interaction energies calculated with Model(3) against SAPT(DFT) energies both before and after relaxation. The excellent performance of the unrelaxed Model(3) is evident. At no stage in the development of Model(3) were the total interaction energies from Dataset(1) included; rather we only used the charge-transfer energies in the development of this model. Additionally, none of the low-energy dimers in Dataset(2) were used in any way in the construction of Model(3), yet these energies are accurately predicted by the unrelaxed Model(3), with very few outliers. This model may be improved by relaxing it to the dimer energies in both data sets. This relaxation was performed with the anisotropic terms in the potential frozen and only the isotropic parameters, including the low-ranking dispersion coefficient, allowed to vary with tight anchors imposed (see the SI for additional information). As seen in Figure 6, this relaxed model exhibits an excellent correlation with the SAPT(DFT) reference energies, and has fewer low energy outliers compared with the unrelaxed model. In the remainder of this paper by ‘Model(3)’ we will refer to this relaxed model.

Similar figures for Model(1) and Model(2) can be found in the SI. As may be expected from the r.m.s. errors reported in Table I, the performance of the unrelaxed Model(1) is excellent given the simplicity of the model, but the unrelaxed Model(2) shows somewhat larger errors for the most strongly bound dimers. However, both of these models improve considerably on relaxation.

In Table I we also report r.m.s. errors for a model functionally identical to Model(3), but created using the DF-AIM approach and with DMA4 multipoles. Apart from these two differences, this model, termed Model(3)-DF-DMA4, has been created in an identical manner to the others reported in this paper. This is the kind of model that might have been created using the approach we have described in an earlier paper on atom-atom potentials[15]. We see that across the $-20 : 20 \text{ kJ mol}^{-1}$ energy range the r.m.s. errors made by this model are twice as large as those from Model(3). This is mainly a consequence of the unphysical AIM atoms that result from the DF-AIM approach that are shown in Figure 1. This approach results in the wrong atomic anisotropies that the fit cannot correct with the limited amount of SAPT(DFT) data in Datasets (1) and (2). This is an inevitable consequence of the Bayes-like approach we have adopted: the role of the first step in the fitting process — the first-order fits through the distributed density overlap model — is to determine prior values for the fitting parameters (see §3 in Part I). The subsequent relaxation steps merely refine these prior values. However, if the prior values are very poor, as they are with the DF-AIM

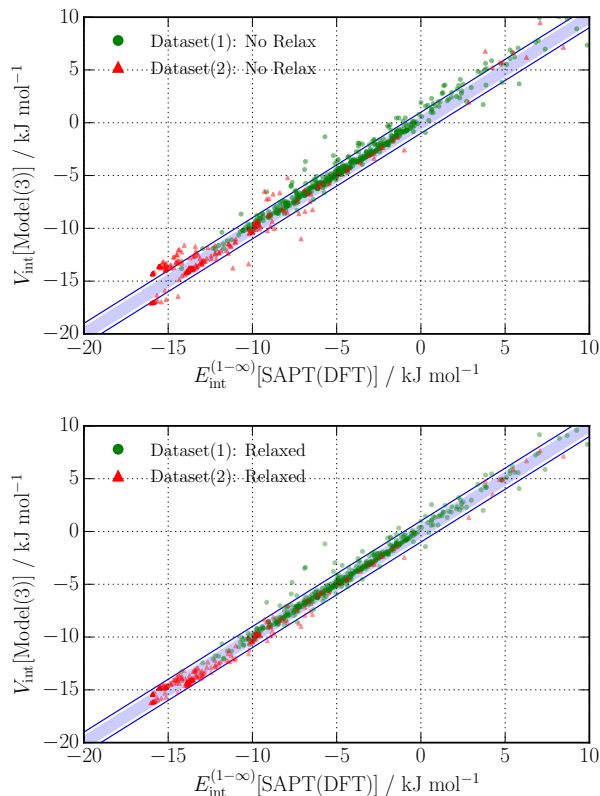


FIG. 6: The total interaction energy models for Model(3). The upper panel shows energies from Model(3) before relaxation to the dimers in Dataset(1) and Dataset(2), and the lower panel shows model energies after relaxation. In both cases these energies are plotted against the total SAPT(DFT) interaction energy $E_{\text{int}}^{(1-\infty)}$. The blue bar represents the $\pm 1 \text{ kJ mol}^{-1}$ deviation from SAPT(DFT).

approach, then we require a considerable amount of data to move them to the correct values. This is not needed with the ISA-based AIM approach, and demonstrates the superiority of this method.

V. RESULTS

A. Minima

We have used the basin-hopping algorithm (see Ref. 16 for a review) as implemented in the ORIENT program to search for stable dimers on the potential energy surfaces. In contrast to the rather simple PES of the benzene dimer [9, 17] which supports only three minima, we have found eight minima for the pyridine dimer. The minimum-energy structures, which are illustrated in Figure 8, may be classified according to their bonding:

- Hydrogen-bonded: These include Hb1, Hb2 and Hb3. Of these, Hb1 is doubly hydrogen-bonded and has been found in a DFT-D (BLYP+Grimme D1 correc-

tion) search [18] and has also been investigated at the CCSD(T)/CBS level of theory [19] to be around $-15.5 \text{ kJ mol}^{-1}$ (estimated from Figure 5 in Ref. 19). This compares well with our SAPT(DFT) energy of $-16.6 \text{ kJ mol}^{-1}$. The Hb2 and Hb3 structures do not appear to have been reported in prior literature.

- Stacked: The S1 and S2 minima are the stacked dimers which are largely dispersion-bound. Both these structures have been found in the DFT-D search, however we see no evidence of the two other stacked structures reported in that study.
- T-shaped: None of these minimum energy dimers are exactly T-shaped, but the T1 and T2 minima are nearly so, and the bT minimum is a very bent-T-shaped structure. The bT structure is similar to one of the T-shaped structures found in the DFT+D search. We do not find the ‘T-shaped 1’ structure in the DFT+D search by Piacenza and Grimme [18].

The minimum configurations are displayed in Figure 8 and their energies are reported in Table II and displayed visually in Figure 9. For comparison, we have calculated SAPT(DFT) interaction energies for the dimer configurations obtained from the relaxed Model(3) PES. Not all of the models support all the minima. Model(2) does not support the Hb3 minimum, which instead relaxes to the T1 structure on this model PES. The relaxed Model(3)-DF-DMA4 supports only five of the eight minima, and two of those (S2 and T1) differ in structure from the corresponding structures on the ISA-based surfaces: in the S2 structure on this surface the molecules are not parallel, and the T1 is bent. The three missing structures relax to either the Hb2 or the T1 structures. The Hb2 minimum is the global energy minimum on this PES.

For Model(3) we have reported energies for the minima on both the unrelaxed and relaxed models. These largest energy differences in the minima on these two PESs differ by just over 1.1 kJ mol^{-1} (just over 7% of the interaction energy). This is a remarkable result as it indicates that the unrelaxed models can be predictive without the need for fitting to the SAPT(DFT) total interaction energies, in particular, no information about total interaction energies of the stable, low-energy dimers was used in creating the three unrelaxed models. Further, the similarity of the relaxed and unrelaxed models suggests that the procedure used here appears to be free of artifacts usually introduced by fitting procedures, and is robust to the inclusion of additional data. However this data needs to be biased to low energy dimers, as has been noted above. We will explore this issue in a forthcoming paper [20].

The agreement between the ISA-based models (relaxed and unrelaxed) is made even clearer in Figure 7 where we display PES sections at representative minima. The agreement between SAPT(DFT) and all models — including the unrelaxed Model(3) — for the minima is generally very good, both in the overall shape of the PESs and the location and depth of the radial minimum. Plots for the remainder of the minima can be found in the SI.

In Table III we report the lowest harmonic vibrational frequencies at these minima. These frequencies give us an indi-

TABLE I: R.m.s. errors (kJ mol^{-1}) for the total interaction energy models for the pyridine dimer. Errors are calculated against SAPT(DFT) total interaction energies, and are reported both for the models relaxed to the set of SAPT(DFT) energies in Dataset(1) and Dataset(2), and for the models obtained by combining the different terms in the potential as described in the text. The errors for these unrelaxed models are reported in parantheses. Model(3)-DF-DMA denotes a model functionally similar to Model(3) but created using the DF-AIM approach with multipoles from the DMA4 model.

Energy range	Model(1)	Model(2)	Model(3)	Model(3)-DF-DMA4
$E \leq -10$	0.59 (1.26)	0.59 (1.22)	0.53 (1.08)	0.97 (1.85)
$-10 < E \leq 0$	0.80 (0.99)	0.72 (0.95)	0.56 (0.70)	1.21 (1.39)
$0 < E \leq 20$	1.69 (2.71)	1.19 (2.58)	0.95 (1.53)	2.17 (3.16)

cation of how different the shapes of the three PESs are at the stable minima configurations. There is generally a good agreement between the minima on all ISA-based models, but the frequencies seem to vary more with the models than the corresponding energies. This may reflect the importance of the anisotropy in determining the shape of the PES. This agreement, though imperfect, is reassuring as it gives us some confidence that the minima we observe are real and not artifacts of the fitting function used. The largest differences are between the ISA-based models and the DF-based Model(3)-DF-DMA4. The lowest vibrational frequencies of the Hb1 and S1 minima are only half as large as the corresponding frequencies for Model(3), indicating that the shape of the PES of Model(3)-DF-DMA4 differs from that of Model(3) in the regions of these minima. This should not be a surprise given the rather significant differences in the AIM shapes from the ISA- and DF-based density partitioning schemes as shown in Figures 1 and 2.

B. Second virial coefficients

The second pressure virial coefficient $B(T)$ represents a necessary, but not sufficient, test of the quality of the two-body PES. As the virial coefficients average over the PES, it is possible to construct an infinity of PESs that yield the correct values of $B(T)$ in a finite temperature range. Nevertheless, it is important that any model PES reproduces the experimental values as a minimum requirement. In Figure 10 we display second virial coefficients calculated for the pyridine dimer. We have calculated $B(T)$ at a range of temperatures using the ORIENT program. Only the Classical results are presented as the quantum corrections were found to be insignificant over the range of temperatures reported here. We used a stochastic integration sampling algorithm with 102 radial steps and 262,144 dimer orientations in order to integrate $B(T)$ sufficiently accurately. From Figure 10 we see that all three models show good agreement with the experimental data of Andon *et al.* [22] and Cox & Andon [23]. As the models all slightly overestimate $B(T)$ across the temperature range of the figure, they may, on the whole, be somewhat too attractive. We will return to this issue later in this paper.

VI. ANALYSIS & DISCUSSION

A. Polarization damping revisited

In developing the damping model for our polarizability models in §5.2 in Part I we recognised an uncertainty in our choice for damping model. This arose because the damping parameter β_{pol} depends on the choice of dimer configurations used to determine it. Here we re-examine this issue by assessing the damping models against data obtained at the eight minimum energy dimer orientations at various separations. In Figure 11 we compare the second-order polarization energies from the polarization models described in §5.2 with second-order polarization energies from regularised SAPT(DFT), $E_{\text{POL}}^{(2)}$. It should be apparent that while our choices for the damping models are reasonable, with errors typically less than 1 kJ mol^{-1} for the attractive dimers, there is a systematic over-damping, with the polarization energies of some (repulsive energy) dimers underestimated by as much as 2.5 kJ mol^{-1} . This problem can be largely remedied by increasing the value of β_{pol} . In the same figure we also display polarization energies calculated with the anisotropic L2 polarization model with $\beta_{\text{pol}} = 1.0 \text{ a.u.}$ This small increase causes a significant improvement to the match between the model and $E_{\text{POL}}^{(2)}$.

In this manner, we are able to determine a new set of models with the appropriate polarization damping chosen self-consistently. As we emphasised in §5.2, the choice of β_{pol} does not affect the quality of the two-body potential. Indeed, Model(3) with this change to the damping is nearly identical in every respect to the original model. The effects will however be manifest in the many-body polarization energies. We are currently investigating this issue.

B. Multipole model rank reduction

Our simplest model, Model(1), contains anisotropic terms only in the ISA-DMA multipole and the polarization models. In §5.1 in Part I we have argued that the ISA-DMA model shows better convergence properties than the usual DMA procedure of Stone [24]. Based on that discussion and the results presented in Figure 1 in Part I, we may ask whether we can truncate the rank of the ISA-DMA model without incurring a

TABLE II: Interaction energies (kJ mol^{-1}) of the pyridine dimers at the energy minima reported in Figure 8. The SAPT(DFT) reference energies have been calculated at the dimer geometries obtained on the relaxed Model(3) PES. The energies reported for all models are for the stationary points on the model PES, therefore the dimer geometries at which the energies are evaluated will depend on the model and will differ from the geometries used to obtain the SAPT(DFT) reference energies. Where a structure is not supported as a minimum we report in parentheses the structure it relaxes into. Thus Model(2) does not support the Hb3 structure which instead relaxes to the T1 minimum on this PES. Structures on the Model(3)-DF-DMA4 surfaces that are only approximately the same as those on the other surfaces are indicated by an asterisk.

Minimum	SAPT(DFT)	Model(1) Relaxed	Model(2) Relaxed	Model(3)		Model(3)-DF-DMA4	
				No Relax	Relaxed	No Relax	Relaxed
Hb1	-16.67	-16.11	-16.00	-17.28	-16.37	-14.38	-15.04
S1	-16.22	-15.64	-15.55	-14.54	-15.61	-13.60*	-15.46
S2	-15.45	-15.38	-15.38	-14.17	-15.35	-12.71*	-14.42*
T1	-14.57	-14.54	-14.73	-14.65	-15.02	-14.63	-14.84*
T2	-14.70	-14.54	-14.69	-14.68	-14.92	(Hb2)	(Hb2)
Hb2	-14.70	-15.03	-14.65	-14.57	-14.76	-15.19	-15.61
bT	-14.01	-14.00	-14.12	-13.97	-14.25	(Hb2)	(Hb2)
Hb3	-13.84	-14.60	(T1)	-13.88	-14.08	-14.00	(T1*)

TABLE III: Lowest harmonic vibrational frequencies for the minima on the relaxed model PESs. For Model(3) we also include data for the unrelaxed version of this model. Model(2) does not support the Hb3 minimum. All frequencies are reported in cm^{-1} .

Minimum	Model(1) Relaxed	Model(2) Relaxed	Model(3)		Model(3)-DF-DMA4	
			No Relax	Relaxed	No Relax	Relaxed
Hb1	15.96	12.76	15.79	15.08	7.01	7.70
S1	6.04	3.83	4.79	6.69	1.94	3.42
S2	9.99	10.53	8.98	11.24	9.60	11.81
T1	3.74	4.45	9.57	6.62	5.37	8.22
T2	1.94	3.89	7.38	6.07	—	—
Hb2	12.05	9.94	12.15	12.19	11.92	10.91
bT	5.55	7.43	3.13	6.28	—	—
Hb3	12.07	—	11.36	10.88	6.88	—

significant loss in accuracy. In Figure 12 we display interaction energy profiles for Model(1) using the ISA-DMA model at various ranks. As before, these calculations have been performed at two representative dimer orientations: Hb1 and S1. At the doubly hydrogen-bonded Hb1 orientation there is no appreciable change on reducing rank to $l = 3$, but any further reduction results in a significant change in the PES with the interaction energy getting systematically smaller (in magnitude). At the dispersion-bound S1 orientation there is almost no change to the model when the rank of the multipole expansion is reduced all the way to $l = 0$ (charges only). This is perhaps to be expected as the electrostatic interaction is relatively insignificant for the S1 (and S2) complexes. What is surprising is that the T1 complex also shows a relative insensitivity to the rank of the multipole expansion.

The behaviour of the models at the doubly-hydrogen-bonded Hb1 dimer configuration needs some explanation. The rank of multipoles on the hydrogen atoms do not appear to matter as the model interaction energies do not alter significantly if only rank 0 (charge) terms are included on these atoms. However, the nitrogen and carbon atoms appear to need the octopolar terms to model the electrostatic interaction cor-

rectly in this configuration. At least for the nitrogen atom this should not be surprising as the octopolar terms are needed to describe the effects from the lone pairs, but it is surprising that the carbon atoms also require these terms. In any case, it may be possible to improve the quality of the charge-only model by including additional sites around the nitrogen and carbon atoms to account for these terms in much the same way as is done for the oxygen atom in water models. If successful, this would provide us with a route to construct a fully isotropic interaction model for pyridine and other systems. This would be important as, with some exceptions such as the ORIENT and DMACRYS [25] programs, simulation programs cannot normally use potentials with anisotropic terms, a restriction that significantly limits the usage of the accurate potentials we are able to develop.

VII. CONCLUSIONS & DIRECTIONS

We have described a robust and relatively easy to implement algorithm for developing accurate intermolecular potentials in which most of the potential parameters are de-

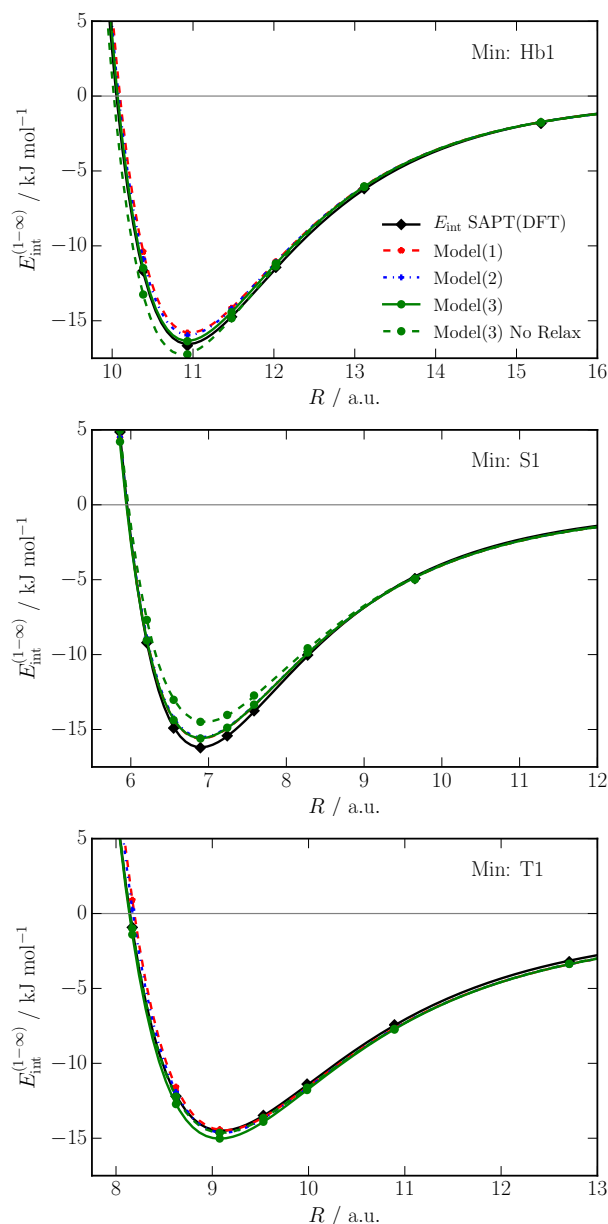


FIG. 7: PES sections at the Hb1, S1 and T1 dimer orientations. Sections at the other minima are provided in the supplementary information.

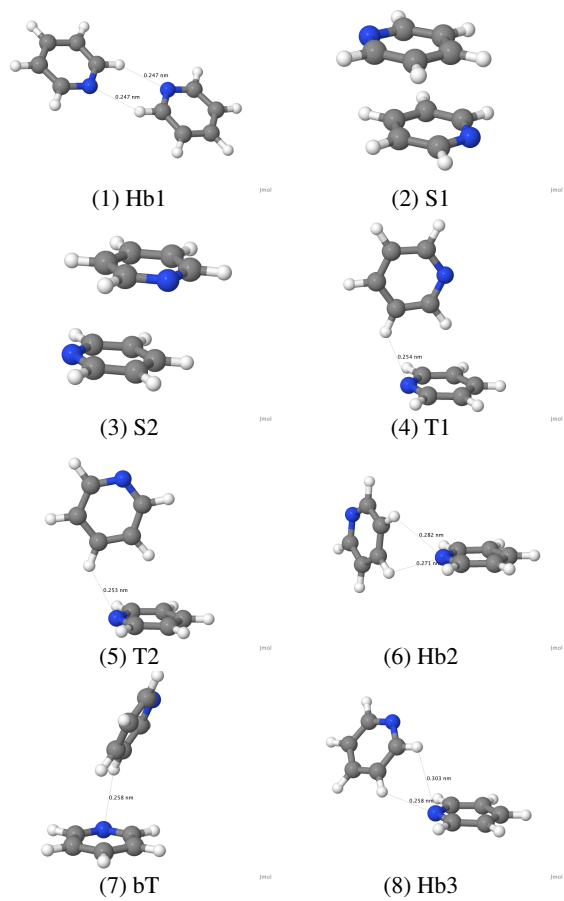


FIG. 8: Structures of pyridine dimers at stable minima on the three PESs. The structures are ordered according to their energies calculated using SAPT(DFT). These images have been produced using the Jmol program [21].

rived from the charge density and density response functions, and the remaining, short-range, parameters are robustly determined by associating these with specific atom-pairs using a basis-space implementation of the iterative stockholder atoms (ISA) algorithm. With this algorithm, accurate, many-body potentials can be derived using a relatively small number of dimer energies calculated using SAPT(DFT). This significantly reduces the computational cost of the approach. Importantly, as all of the long-range and most of the short-range parameters are *derived*, the predictive power of the resulting potentials is significant.

One of the major obstacles to intermolecular potential development has been the derivation of the short-range parameters. We have demonstrated that these can be relatively easily and robustly derived from the non-interacting charge densities using the distributed density-overlap model based the ISA. In this manner, even the atomic anisotropy terms, which are usually poorly defined in a direct fit, are robustly determined with a relatively small amount of computational effort. Using these techniques on the pyridine dimer, we have demonstrated that features such as the density distortions due to the π -bonding

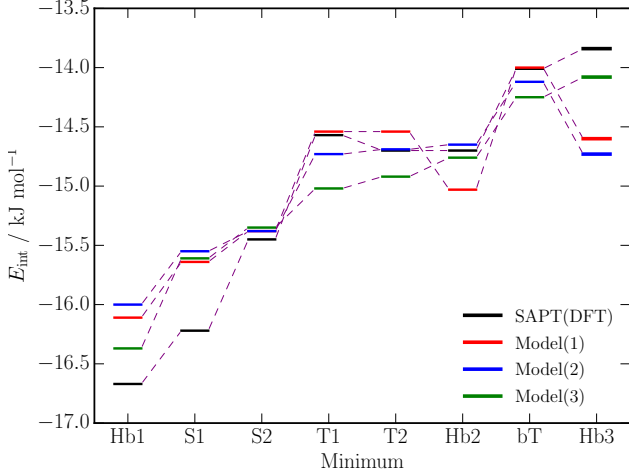


FIG. 9: Visualisation of the data in Table II. The energies of stable dimers on the three PESs are displayed as solid horizontal bars. The dashed lines link the energies levels associated with each of the three models. SAPT(DFT) reference energies have been calculated at the dimer geometries from Model(3). Data for Model(3)-DF-DMA4 are not shown here.

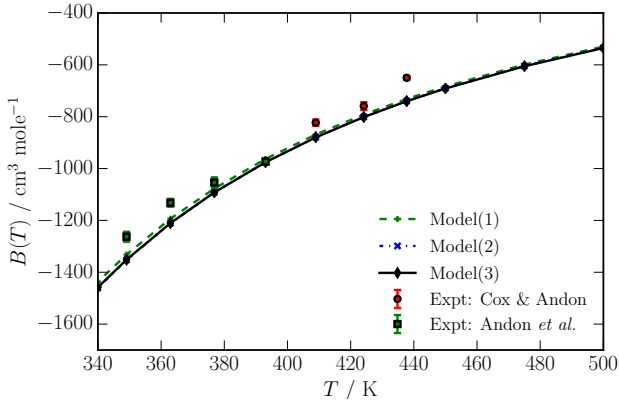


FIG. 10: Classical second virial coefficients for pyridine. The experimental data and error bars are from Andon *et al.* [22] and Cox & Andon [23]. Quantum corrections contribute very little and would not make a visible difference on the scale of this graph.

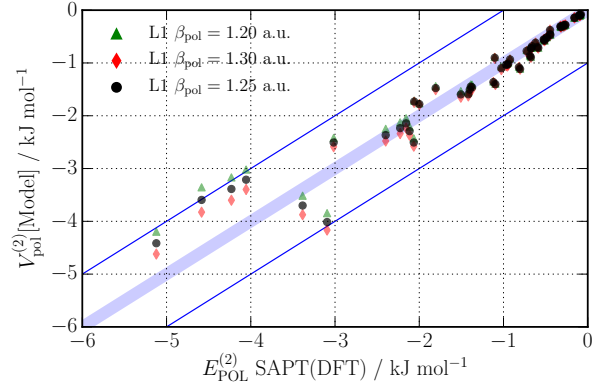


FIG. 11: Second-order polarization energies from regularised SAPT(DFT) compared with the L1 polarization model. The energies have been calculated using minimum energy dimer configurations obtained on the Model(3) PES. Dimers with attractive total interaction energies are indicated with filled symbols, and those with repulsive energies with open symbols. The thin blue lines indicate the ± 1 kJ mol⁻¹ error limits and the blue bar is present just as a visual aid.

on the carbon atoms, and the lone pair on the nitrogen atom in pyridine are well-defined using our approach. Indeed, only terms with a physical origin are present in this approach.

The main features of the methodology we describe in the paper are:

- *Efficient use of data:* The potentials are derived using a hierarchy of data sets; the more extensive data sets include only first-order energies and can be very easily calculated, while the second-order energies are included through a significantly smaller data set.
- *Priors:* We use the first and most extensive data set to determine prior values for most of the short-range parameters. These priors may subsequently be modified using the second, smaller data set. These steps may be repeated thus leading to a multi-stage procedure which significantly reduces the amount of data needed to tune the potential.
- *ISA:* The short-range parameters are determined using the ISA method for partitioning the molecular densities into atomic contributions. The BS-ISA algorithm allows this to be performed using extensive basis sets with a well-defined basis set limit. The ISA atoms are as close to spherical as is possible and account for charge movement within the molecule, consequently the resulting short-range repulsion parameters may be expected to be free from basis set artifacts, and be the most isotropic possible. This compares favourably with the density-fitting-based partitioning scheme we have proposed in earlier papers [8, 15] which does not fulfil either of these properties. Indeed the r.m.s. errors made by the ISA-based models are half as much as those from the density-fitting-based models.

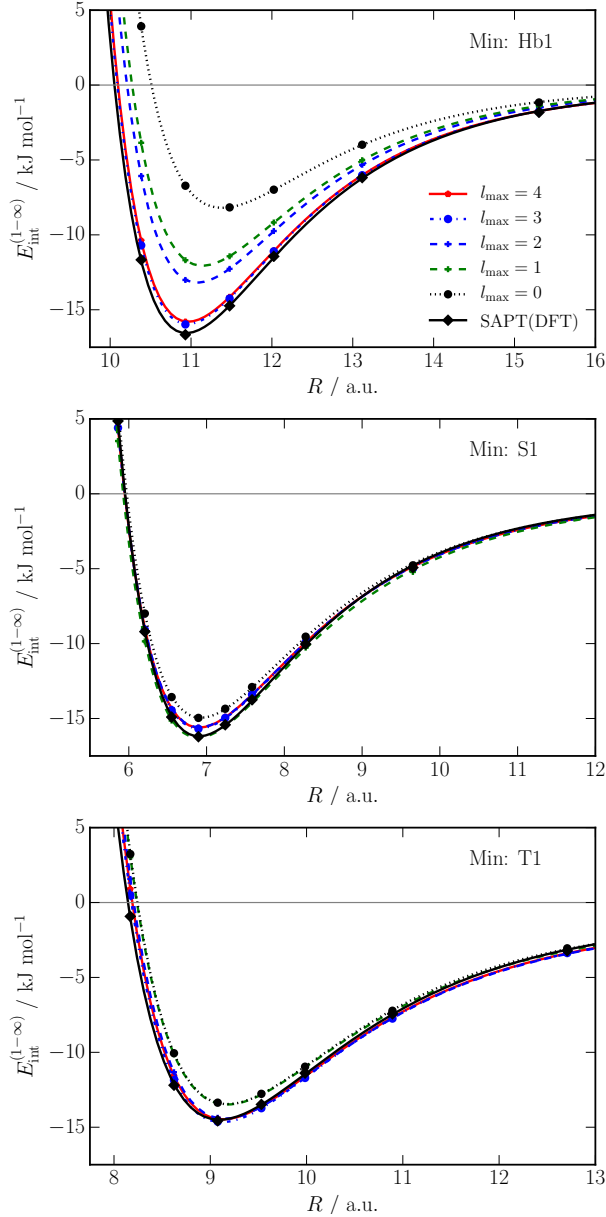


FIG. 12: The effect of rank reduction of the multipole model for Model(1).

- *Long-range models:* The long-range parameters of the potentials are determined using distributed multipoles, polarizabilities and dispersion coefficients. The ISA-DMA multipoles are obtained from the BS-ISA approach and have been demonstrated to exhibit systematic convergence with rank. The WSM distribution scheme has been used to calculate the distributed polarizabilities and dispersion coefficients, the latter of which we have tuned to SAPT(DFT) dispersion energies.
- *Predictive power:* Most of the parameters are derived from or fitted to molecular properties, consequently they are physically meaningful and the resulting potentials exhibit a considerable predictive power.
- *Hierarchy of models:* The methods we have described allow us to determine potentials of various levels of complexity in a meaningful manner. These may be fully isotropic at the atom-atom level or contain as much anisotropy as is needed.

We have used these techniques to develop a set of potentials of varying levels of detail for the pyridine dimer. The simplest of these include only isotropic short-range terms, and the most detailed includes all significant anisotropy terms up to rank two. The predictive power of these potentials is quite significant and all are able to predict SAPT(DFT) interaction energies for low energy dimers not included in the fit. As a consequence, the potentials are robust to the inclusion of additional data: parameters alter very little on relaxation, and features on the potential energy landscape change only slightly. This robustness is particularly important in the development of multidimensional potentials, as we will generally be unable to sample dimer configuration space adequately, especially for larger monomers.

We have compared our newly derived pyridine potentials to the rather limited set of data available in the literature. Of the eight stable minima found on the Model(3) PES, the double hydrogen-bonded Hb1 dimer has been found in previous DFT+D work by Piacenza and Grimme [18], and the CCSD(T) energy for this structure [19] differs from our SAPT(DFT) interaction energy by only 7%. The two other hydrogen-bonded structures, Hb2 and Hb3, have not been seen before. Both the stacked structures, S1 and S2, have been found earlier [18]. Of the three T-shaped structures, only the bT structure resembles a previously found structure [18], while the T1 and T2 structures appear to be unique to the models developed in this paper. As the DFT+D method cannot be relied on to correctly describe the subtle balance of dispersion, electrostatic, polarization and charge-transfer interactions seen in the eight dimers of pyridine, it is possible that the set of eight minima we have found are a more accurate representation of this system. Further tests are needed at the CCSD(T) level of theory if we are to be sure of this.

In this paper we have provided solutions to some of the most significant issues related to potential development, and, as a consequence, have inevitably exposed other minor issues that need resolving. Some of these are:

- The WSM method for deriving distributed polarization and dispersion models is a good one, but it is based on a less than ideal partitioning method [13] that seems to result in some artifacts in the models and a small, but undesirable basis-set dependence.
- The current damping of the dispersion model based on molecular ionisation potentials only is less than ideal and there is good reason to expect a site–site damping model to perform better.
- More needs to be done to understand the origin of the polarization damping. Like the dispersion damping, here too it is clear that the damping model needs to depend on the pair of interacting sites, but there is evidence [4] that the polarization damping differs strongly from that used for the dispersion. This is probably the least understood issue at present.
- The resulting potentials are for rigid monomers only. However, as the potential parameters are closely associated with the properties of the atoms in the interacting molecules through either the ISA or the DF-based partitioning methods, it is possible that these models may be applicable to flexible monomers. This conjecture needs to be tested.
- One of the most serious limitations of the approach we have described here is that there are very few simulation programs capable of using these potentials. Most simulation programs use the simpler Lennard-Jones models with point-charge electrostatic models. However, distributed multipoles are being increasingly available in simulations codes: both OPENMM [26] and DL_POLY [27] allow the use of distributed multipoles and simple polarization models, but only the ORIENT [28] and DMACRYS [25] programs currently support the use of the anisotropy terms present in our more complex potentials. We do not doubt that this situation will change as potential development using the methods described in this paper becomes more streamlined and easy to use, and as we accumulate evidence that these more elaborate potentials do result in higher predictive accuracy.

It should be apparent that the ISA — in particular, the BS-ISA algorithm — plays a central role in the methodology we

have described. Consequently it should come as no surprise that some of the issues listed above may be resolved using data extracted from the ISA atomic densities. In a forthcoming paper [20] we will describe how the dispersion damping issue may be resolved using the ISA, and also how even more of the short-range parameters may be derived rather than fitted.

However, there are issues with the models we have presented here. Second virial coefficients are well reproduced using our isotropic and anisotropic potentials, though all three models give $B(T)$ somewhat too negative. This indicates that the models are somewhat too attractive on the average. We have established that there are indeed regions of configuration space where all potentials systematically overbind and these are associated with stacked-like configurations. While we do not fully understand the origin of the problem, it is possible that the additivity assumption we have made in the definition of ρ_{ab} in eq. (2) is inappropriate, and also that the SAPT(DFT) interaction energies are themselves too attractive for these configurations due to the known problems with the $\delta_{\text{int}}^{\text{HF}}$ term for dispersion-bound systems [29, 30]. We are actively engaged in understanding these issues.

VIII. ACKNOWLEDGEMENTS

AJM would like to thank Prof Sally Price for initiating and motivating this project and supporting it, particularly in its early stages, Dr Richard Wheatley for useful discussions related to the ISA, and Lauretta Schwartz for preliminary work on rank reduction of the multipole model. We would like to thank Mary J. Van Vleet for useful comments on the manuscript. AJM would also like to thank Queen Mary University of London for computing resources, the Thomas Young Centre for a stimulating environment, and the Cambridge University Library for generous resources.

This work was partially funded by EPSRC grant EP/C539109/1.

IX. SUPPLEMENTARY INFORMATION

The SI included with this paper contains details of the three potentials derived in this paper. Additionally, plots referenced but not included in this paper are provided in the SI.

-
- [1] Lillestolen, T. C.; Wheatley, R. J. *Chem. Commun.* **2008**, 2008, 5909–5911.
 - [2] Lillestolen, T. C.; Wheatley, R. J. *J. Chem. Phys.* **2009**, *131*, 144101–6.
 - [3] Misquitta, A. J.; Stone, A. J.; Fazeli, F. J. *Chem. Theory Comput.* **2014**, *10*, 5405–5418.
 - [4] Misquitta, A. J. *J. Chem. Theory Comput.* **2013**, *9*, 5313–5326.
 - [5] Anghel, A. T.; Day, G. M.; Price, S. L. *CrystEngComm.* **2002**, *4*, 348 – 355.
 - [6] Hodges, M. P.; Wheatley, R. J. *Chem. Phys. Lett.* **2000**, *326*, 263–268.
 - [7] Stone, A. J. *The Theory of Intermolecular Forces*, 2nd ed.; Oxford University Press, Oxford, 2013.
 - [8] Misquitta, A. J.; Welch, G. W. A.; Stone, A. J.; Price, S. L. *Chem. Phys. Lett.* **2008**, *456*, 105–109.
 - [9] Totton, T.; Misquitta, A. J.; Kraft, M. J. *Chem. Theory Comput.* **2010**, *6*, 683–695.
 - [10] Nyeland, C.; Toennies, J. P. *Chem. Phys. Lett.* **1986**, *127*, 172–177.
 - [11] Mitchell, J. B. O.; Price, S. L. *J. Phys. Chem. A* **2000**, *104*,

- 10958–10971.
- [12] Piquemal, J.-P.; Cisneros, G. A.; Reinhardt, P.; Gresh, N. *J. Chem. Phys.* **2006**, *124*, 104101–12.
- [13] Misquitta, A. J.; Stone, A. J. *J. Chem. Phys.* **2006**, *124*, 024111–14.
- [14] Patkowski, K.; Jeziorski, B.; Szalewicz, K. *J. Mol. Struct. (Theochem)* **2001**, *547*, 293–307.
- [15] Stone, A. J.; Misquitta, A. J. *Int. Revs. Phys. Chem.* **2007**, *26*, 193–222.
- [16] Wales, D. J. *Energy Landscapes: with applications to clusters, biomolecules and glasses*; Cambridge University Press, Cambridge, 2003.
- [17] Podeszwa, P.; Bukowski, R.; Szalewicz, K. *J. Phys. Chem. A* **2006**, *110*, 10345–10354.
- [18] Piacenza, M.; Grimme, S. *ChemPhysChem* **2005**, *6*, 1554 – 1558.
- [19] Hohenstein, E. G.; Sherrill, C. D. *J. Phys. Chem. A* **2009**, *113*, 878–886.
- [20] Van Vleet, M. J.; Misquitta, A. J.; Stone, A. J.; Schmidt, J. R. **2015**, submitted.
- [21] Jmol: an open-source Java viewer for chemical structures in 3D. 2015; <http://www.jmol.org/>, Accessed: Sep 2015.
- [22] Andon, R. J. L.; Cox, J. D.; Herington, E. F. G.; Martin, J. F. *Trans. Faraday Soc.* **1957**, *53*, 1074–1082.
- [23] Cox, J. D.; Andon, R. J. L. *Trans. Faraday Soc.* **1958**, *54*, 1622–1629.
- [24] Stone, A. J. *J. Chem. Theory Comput.* **2005**, *1*, 1128–1132.
- [25] Price, S. L.; Leslie, M.; Welch, G. W. A.; Habgood, M.; Price, L. S.; Karamertzanis, P. G.; Day, G. M. *Phys. Chem. Chem. Phys.* **2010**, *12*, 8478–8490.
- [26] Eastman, P.; Friedrichs, M. S.; Chodera, J. D.; Radmer, R. J.; Bruns, C. M.; Ku, J. P.; Beauchamp, K. A.; Lane, T. J.; Wang, L.-P.; Shukla, D.; Tye, T.; Houston, M.; Stich, T.; Klein, C.; Shirts, M. R.; Pande, V. S. *J. Chem. Theory Comput.* **2013**, *9*, 461–469.
- [27] Todorov, I. T.; Smith, W.; Trachenko, K.; Dove, M. T. *J. Mater. Chem.* **2006**, *16*, 1911–1918.
- [28] Stone, A. J.; Dullweber, A.; Engkvist, O.; Fraschini, E.; Hodges, M. P.; Meredith, A. W.; Nutt, D. R.; Popelier, P. L. A.; Wales, D. J. ORIENT: a program for studying interactions between molecules, version 4.8. University of Cambridge, 2016; <http://www-stone.ch.cam.ac.uk/programs.html\#Orient>, Accessed: May 2016.
- [29] Podeszwa, R.; Szalewicz, K. *Chem. Phys. Lett.* **2005**, *412*, 488.
- [30] Patkowski, K.; Szalewicz, K.; Jeziorski, B. *J. Chem. Phys.* **2006**, *125*, 154107.